A method for increasing depth of field during droplet imaging

J. R. Saylor and B. K. Jones
Clemson University, Clemson, South Carolina 29634

L. F. Bliven
NASA, Goddard Space Flight Center, Wallops Island, Virginia 23337

(Received 12 November 2001; accepted for publication 11 March 2002)

The measurement of water drops using direct optical imaging involves a tradeoff between the camera depth of field and the accuracy of the measured droplet size. A large depth of field increases the length of that portion of the optical axis that is in focus. However, since drops closer to the camera appear larger than those farther away, increasing the depth of field also increases errors in the measured drop size unless *a priori* knowledge exists concerning the location of the drop along the optical axis. Herein a method is presented for ascertaining drop location using a single camera. The method uses a characteristic of the droplet image which is observed when droplets are illuminated from behind. Once the location of the droplet is obtained, the appropriate magnification ratio is applied, permitting an accurate droplet size measurement. This method has been tested on glass spheres of various size. The relevance of this work to precipitation science is discussed. [DOI: 10.1063/1.1475353]

I. INTRODUCTION

Many techniques exist for measuring the size of a liquid drop. However, when information concerning both the drop size and shape is required, direct optical imaging is necessary (while interferometric methods do exist that provide information regarding drop shape, these methods have limits, and interpretation of the data is problematic[1,2]). In this discussion, direct optical imaging refers to the process of creating an image of a drop, or group of drops, using a lens and projecting this image onto a photographic film, or more typically, a charge coupled device (CCD) detector. Once the size of the drop image is obtained it can then be related to the size of the actual drop using the magnification ratio of the lens assembly M:

$$M = \frac{d'}{d}, \tag{1}$$

where d is the diameter of the drop and d' is the diameter of the drop in the image.[3]

While the results presented here find application in several areas of aerosol science, the main motivation for this work concerns the study of rain. Global measurements of rain rate are now becoming feasible due to the development of a network of satellite and ground-based precipitation radars.[4] These radars obtain rain rate by measuring the backscattered intensity of a radar beam as it travels through a collection of falling raindrops. Raindrops exhibit a range of sizes due to coalescence and breakup mechanisms,[5–7] and shapes due to deformation and shape oscillations.[8–11] The radar energy backscattered from a given drop is a function of both size and shape, and hence a knowledge of the raindrop size and shape distributions is critical. The understanding of these distributions is presently incomplete, and significant errors in radar measurements of rain rate exist as a result.[12] Accordingly, the measurement of raindrop size and shape is an active area of research in precipitation science.

Several methods exist for raindrop measurement. The Joss–Waldvogel disdrometer obtains drop size by measuring the displacement of a styrofoam cone as it is impacted by rain drops.[13,14] This is perhaps the most commonly used device, however, it only measures drop size and provides no information concerning drop shape. A disdrometer capable of both size and shape measurement is the two-dimensional (2D) video disdrometer, manufactured by Joanneum Research.[15] This device uses two line scan cameras to obtain perpendicular projections of a droplet falling through two, parallel sheets of white light. The line scan cameras measure the size and shape of the drop by measuring the portion of the light sheet occluded by the falling droplet. Since the raindrop image is acquired in sequential planar sections as it falls through the light sheet, horizontal motion of the droplet results in an excessively oblate and canted drop image.[16] This is a significant problem since droplets frequently have a horizontal velocity due to the winds which accompany rain storms. Algorithms have been developed to account for this error, but have been limited in their success.[17] Another device which measures both drop size and shape is the particle measuring systems probe (now manufactured by Particle Metrics, Inc.). This 2D precipitation monoprobe obtains an occulted image of the drop by focusing a HeNe laser beam to a small measurement volume just in front of a linear photodiode array. The HeNe laser is directed at the photodiode array, and drops which pass through the measurement volume occlude a portion of the linear array. Successive scans of the array are used to reconstruct a 2D droplet image in much the same way as for the 2D video disdrometer described above. This system has been used by many researchers (e.g., Chandrasekar *et al.*[18] and Yuter and Houze[19]). The PMS probe is typically mounted on an aircraft platform

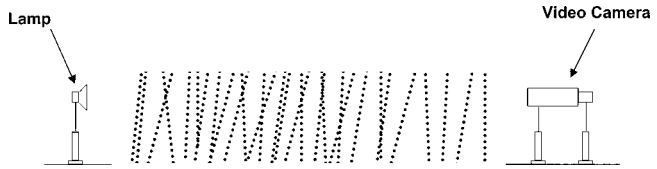

FIG. 1. Illustration of the RIS system.

where the velocity of the aircraft effectively creates a large measurement volume by sweeping the relatively small measurement area through a large number of droplets. This has the disadvantage of blurring over spatial differences that exist in rain storms since large regions are quickly traversed by the aircraft.

To address the shortcomings of the systems described above, Bliven[20] developed a system that images raindrops as they are back-lit from an ordinary white light source. This system, referred to as the rain imaging system (RIS), is illustrated in Fig. 1. It consists of a CCD camera which acquires images at video rates, and a white light source, both located on a single optical axis. A 220 mm focal length lens is mounted on the camera and is focused midway between the camera and light source. The camera and light source are separated by 4 m. Drops which fall within the depth of field of the camera are imaged and transferred to a frame-grabber on a PC. Pattern recognition software is used to identify drops and record their size and shape in real time. This is the first automated system, to the authors' knowledge, which measures raindrops by direct optical imaging.

A sample image of a falling water drop acquired by the RIS system is presented in Fig. 2. Because the drop is illuminated from behind, the image consists of a dark shadow with a clearly defined outline, and a bright spot in the center of the drop. The bright spot is the image of the light source, as seen through the drop (the light source used here was rectangular in shape). The bright central spot is used for several functions in the RIS system. First, the high contrast between the bright spot and the dark shadow permits efficient pattern recognition and is therefore used to identify the existence of the drop. Second, because drops located outside of the depth of field do not display this bright spot, rejection of objects that do not have this spot eliminates out of focus drops, resulting in a well-defined measurement volume. Finally, particles other than raindrops (e.g., dust, leaves, insects, etc.) do not have bright spots in their center, and rejection of these images insures that only raindrops are recorded. Although the existence of the bright spot illustrated in Fig. 2 has been observed by other researchers,[21,22] its use in drop sizing has not been investigated.

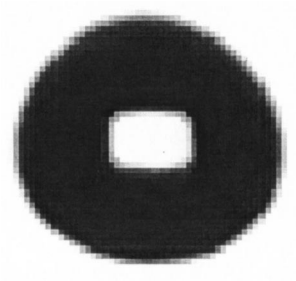

FIG. 2. Sample image of a falling drop obtained using the RIS system. The drop is 2.7 mm in diameter.

Drop size distributions evolve during the course of a storm. To accurately measure this evolution, the number of raindrops which are recorded per second should be large so that accurate distributions can be computed using data obtained over short time intervals. For a given rain rate, the number of droplets measured by a disdrometer is determined by its measurement volume. For the RIS system, the measurement volume is determined primarily by its depth of field (the area imaged can also be increased, but this would reduce the spatial resolution, causing small drops to be missed). In its present configuration, the RIS system has a 17 cm depth of field. Increasing this depth of field is easily achieved by reducing the iris size (increasing the $f/\#$). However, as the depth of field is increased, errors in the measurement of the drop size are incurred; drops near the camera create a larger image than those farther away. Stated another way, the correct magnification ratio M [Eq. (1)] depends on the location of the drop along the optical axis of the camera z_d. The purpose of the research presented here is to develop a method for determining z_d from information gleaned solely from the drop image. Such information would allow the drop location to be determined without resorting to complex methods such as stereographic imaging.[23]

In addition to precipitation research, the measurement of liquid drop sizes is relevant to many engineering applications where liquid drops exist in a gas flow. For example, in nuclear reactor cooling two-phase flows are common, and measurements of the distribution of liquid droplet sizes is important. In the area of internal combustion engines and gas turbines, fuel is atomized into a liquid spray, and measurements of the resulting droplets are needed. And, in agricultural applications the efficacy of insecticide and herbicide deposition relies on the characteristics of the liquid spray. The methods used to measure drop characteristics in these different situations are many and diverse, and descriptions can be found in reviews by Chigier.[24,25] Some of these methods rely on direct optical imaging and hence will also benefit from the work presented here.

The organization of this article is as follows. In Sec. II, the experimental method used to study characteristics of the droplet image is described. In Sec. III, the results obtained from these experiments are presented. The method by which these results can be used to increase the depth of field of an imaging system without increasing sizing errors is discussed in Sec. IV.

II. EXPERIMENTAL METHOD

In Fig. 3 the experimental setup used for this work is presented. The system consists of a CCD video camera fitted with a 220 mm lens, a 150 W halogen lamp, and a PC with data acquisition and image processing software. This setup is identical to the RIS system described by Bliven[20] except that $f/\#$ and z_l (the distance between the light source and the camera lens) are varied.

For these experiments, spherical glass lenses were used

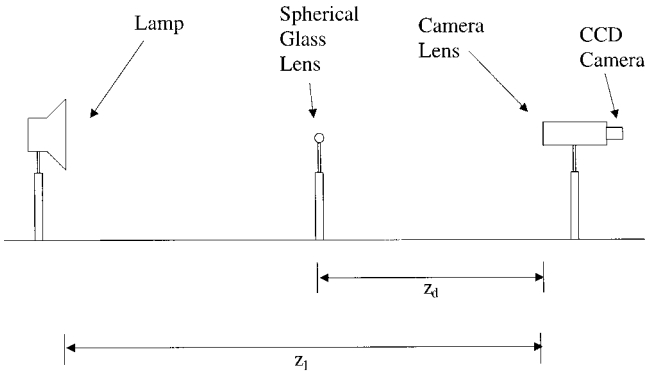

FIG. 3. Schematic illustration of the experimental setup.

instead of actual water drops. These glass spheres were mounted atop a standard optical post and positioned along the optical axis of the system using an optical rail. In this way ''drops'' of known, fixed diameter were imaged without the problems associated with creating reproducible liquid drops. A sample image of such a glass sphere is presented in Fig. 4.

To measure the depth of field, a sequence of images of the glass sphere was obtained. The glass sphere was placed close to the camera and progressively moved away, recording images at discrete locations along the optical axis. The distance between the glass sphere and the camera z_d was recorded for each image. Image acquisition began roughly at $z_d = 160$ cm and ended at $z_d = 255$ cm. Images were acquired every centimeter in regions where the drop image was coming into focus or going out of focus. In other regions these increments were larger, typically 3–5 cm. The range in z_d over which the image was in focus was recorded as the depth of field.

As described in Sec. I, objects were determined to be in focus if a bright spot existed in their center. The existence of a bright spot was determined by first thresholding the 8-bit image to a binary image based on a clustering algorithm. The threshold value was chosen based on the pixel histogram and pixels having a value above the threshold were assigned a value of 1, and those below the threshold were assigned a value of 0. A segmentation algorithm was then used to group pixels that were completely surrounded by pixels having a value different from their own. This function identified the presence of the inner bright spot. If this spot was present the spot width d_s' was recorded. Next, the image was inverted to avoid divide-by-zero errors. In the fourth and final step, the maximum horizontal distance between pixels in the outline was determined and recorded as the outer diameter of the image d'.

TABLE I. Matrix of z_l, d, $f/\#$ combinations that were experimentally investigated.

d (mm)	$f/\#$	$z_l = 260$ cm	$z_l = 330$ cm	$z_l = 400$ cm	$z_l = 470$ cm
10	4	x	x	x	x
10	8	x	x	x	x
10	22	x	x	x	x
8	4	x			
8	8				
8	22	x			
6	4	x			
6	8				
6	22	x			
4	4				
4	8	x	x	x	x
4	22	x	x		

The depth of field was measured for a range of glass sphere diameters d, $f/\#$ settings and values of z_l. The $(z_l, f/\#, d)$ parameter space was

$$z_l = 260, 330, 400, 470 \text{ cm}, \tag{2}$$

$$d = 4, 6, 8, 10 \text{ mm}, \tag{3}$$

$$f/\# = 4, 8, 22. \tag{4}$$

Of course z_d was varied to determine the depth of field for each combination of the above parameters that was investigated. The parameter combinations which were explored are presented in matrix form in Table I. The results of these depth of field measurements are now presented.

III. RESULTS

In Fig. 5 a plot is presented of measured diameter d' vs z_d for a glass sphere having a diameter $d = 10$ mm. These data were obtained using the experimental setup presented in Fig. 3 with $f/\# = 8$ and $z_l = 400$ cm (the standard RIS

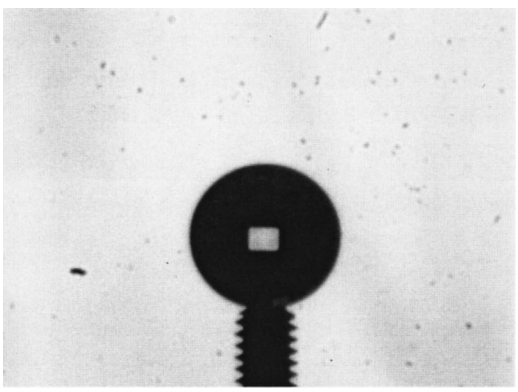

FIG. 4. Sample image of a 10 mm glass sphere. The support beneath the sphere is a small threaded set screw.

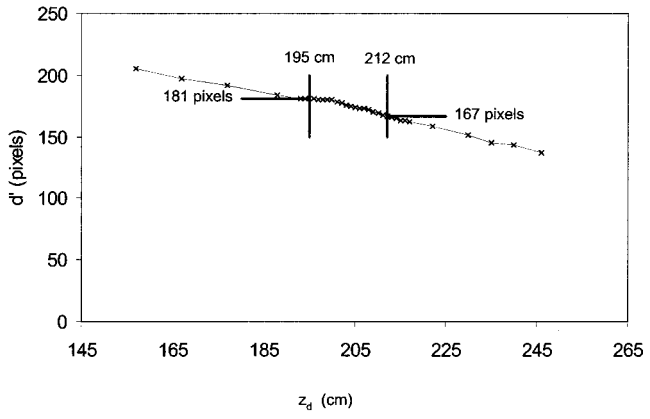

FIG. 5. Plot of d' vs z_d for $d = 10$ mm, $f/\# = 8$, and $z_l = 400$ cm.

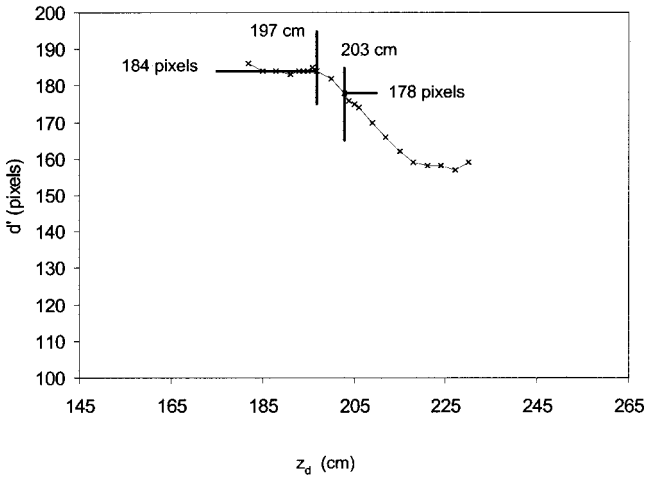

FIG. 6. Plot of d' vs z_d for $d=10$ mm, $f/\#=4$, and $z_l=400$ cm.

configuration[20]). The depth of field is indicated as the region between the vertical bars where the drop image is in focus. The measured depth of field for this configuration is 17 cm. The plot presented in Fig. 5 reveals the error in measured diameter d' caused by having a finite depth of field. At the edge of the depth of field nearest the camera ($z_d=195$ cm), $d'=181$ pixels, while at the edge of the depth of field farthest from the camera ($z_d=212$ cm), the measured image has shrunk to $d'=167$ pixels, a range of 8% (an error of $\pm 4\%$).

Plots of d' vs z_d for $f/\#=4$ and $f/\#=22$ are shown in Figs. 6 and 7, respectively. Figure 6 reveals a reduction in depth of field to 6 cm when the $f/\#$ is reduced to 4, reducing the sizing error to $\pm 2\%$. In Fig. 7 the $f/\#$ is set to 22, and a larger (and more desirable) depth of field of 51 cm is attained, however the sizing error increases to $\pm 11\%$. Similar results were obtained using glass spheres having a diameter of $d=4$, 6, and 8 mm. The depth of field also changes with z_l as revealed by the data presented in Table II.

To make use of the larger depth of field associated with a large $f/\#$, a method for ascertaining the drop location z_d is needed. If z_d is known, an appropriate magnification ratio M can be applied. Such a method would effectively yield the benefits of a large depth of field without the associated error.

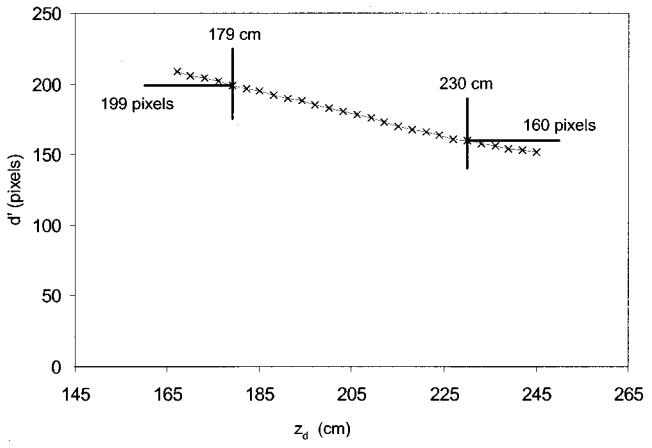

FIG. 7. Plot of d' vs z_d for $d=10$ mm, $f/\#=22$, and $z_l=400$ cm.

TABLE II. Depth of field dimensions for $z_l=260$, 330, 400, and 470 cm ($f/\#=8$).

z_l (cm)	Depth of field (cm)
260	44
330	24
400	17
470	12

Ascertaining z_d from imagery obtained with a single camera requires that some characteristic of the drop image be sensitive to z_d. The ratio of the width of the inner bright spot d_s' to the outer diameter d' has this characteristic. This ratio is referred to as

$$\alpha=\frac{d_s'}{d'}. \tag{5}$$

Figure 8 identifies d_s' and d' for a sample image, and α is plotted against z_d in Fig. 9 revealing a monotonic relationship. Hence there is a unique α for each z_d. Moreover, the α vs z_d plots are independent of diameter. Therefore, once a drop is imaged, α can be computed and z_d obtained from the α vs z_d relationship. Knowing z_d, the appropriate magnification ratio M can be applied to the drop image size d' to provide an accurate drop size measurement d using Eq. (1).

The results presented in Fig. 9 were all for a camera to light source distance $z_l=260$ cm. Figure 10 presents a plot of α vs z_d for $z_l=400$ cm. Here α achieves a maximum value near the middle of the depth of field, and then diminishes as z_d is further increased, signifying that more than one possible z_d value exists for each α at this z_l. This behavior was observed for all $z_l>260$ cm, indicating that the utility of this method is restricted to configurations where z_l is relatively small (i.e., when the camera and light source are relatively close together).

IV. DISCUSSION

The goal of the research presented herein was to develop a method for locating the position of a drop along the optical axis of a camera using information obtained solely from that camera. The results presented in Fig. 9 reveal that this can indeed be done. These data show that once α is computed for a drop, irrespective of its diameter, z_d can be determined. That is, the α vs z_d plot is monotonic and independent of

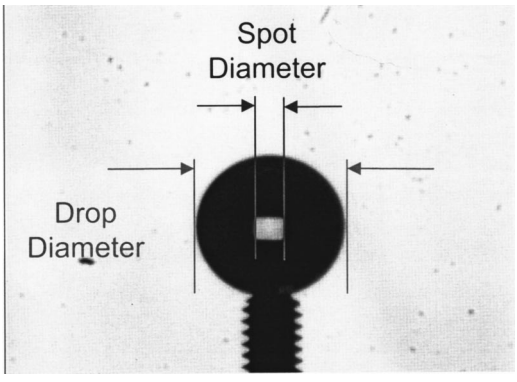

FIG. 8. Sample image presenting the dimensions used to obtain α.

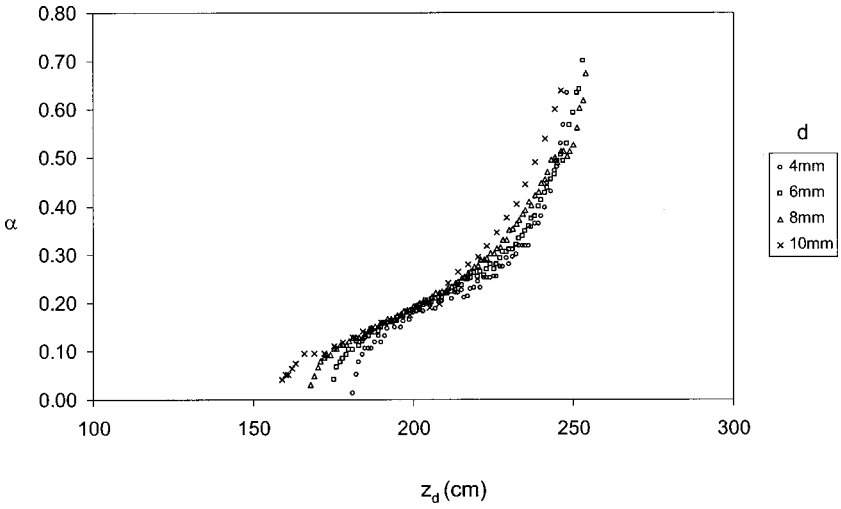

FIG. 9. Plot of α vs z_d for $f/\#=22$, $z_l=260$ cm, $d=4$, 6, 8, and 10 mm.

drop size, at least for the range of diameters investigated (4–10 mm). The monotonic relationship presented in Fig. 9 is significant because it allows droplet sizing to occur using large $f/\#$ optics. Since the magnification ratio M is a function of distance from the camera, once the droplet location is ascertained, the correct M can be applied allowing accurate droplet sizing over a large range of the optical axis.

As noted in the Introduction, this method can be applied to any branch of aerosol science where imaging is used to quantify drop size. Of particular interest here is precipitation science where imaging is used to measure the distribution of raindrop sizes and shapes. This method will permit a larger depth of field to be used in this application. Such a large depth of field allows a larger number of raindrops to be measured per unit time, at any given rain rate. This is particularly useful at low rain rates where a very long measurement time would be required to obtain an accurate drop size distribution if the depth of field was small.

The data presented in the previous section were all for drops centered on the optical axis. To determine how these results might change for off-axis drops, α was remeasured for the 8 mm glass sphere. For $z_d=190$ and 230 cm, images were obtained with the sphere located on the far left, center, and far right side of the field of view. In all cases the value of d' differed by at most two pixels, resulting in a negligible effect on α. Hence, this method works equally well for on-axis and off-axis drops.

The results presented here pertain only to spherical drops. In applications where drops are small (typically sub-millimeter) these results are adequate since surface tension forces maintain the spherical shape at sufficiently small diameters. Large drops, however, tend to oscillate and attain ellipsoidal shapes. A repetition of the experiments presented here for the range of shapes that drops can exhibit goes beyond the scope of this work. However, preliminary experiments along these lines have revealed results similar to those presented in Fig. 9 for a glass ellipsoid having a major-to-minor axis ratio of 1.11, suggesting that this method may work for large, nonspherical drops as well.

It is noted that the results presented here apply only to the smallest camera-to-light source distance which was investigated (260 cm). At larger values of z_l, a monotonic relationship between α and z_d no longer exists and the method fails. Hence the utility of this method is restricted to situations where the camera and light source can be placed reasonably close together.

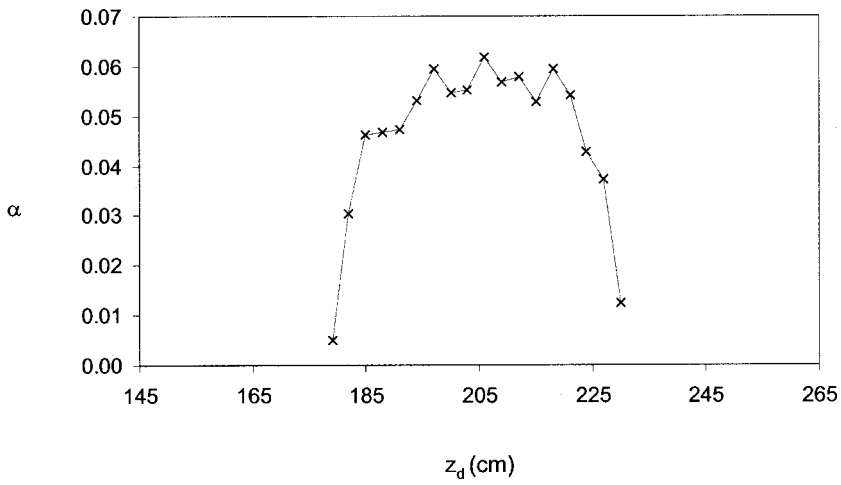

FIG. 10. Plot of α vs z_d for $f/\#=22$, $z_l=400$ cm.

ACKNOWLEDGMENTS

Financial support from the National Science Foundation via the Research Experience for Undergraduates Program is gratefully acknowledged.

[1] D. R. Secker *et al.*, Appl. Opt. **39**, 5023 (2000).
[2] G. Videen *et al.*, Appl. Opt. **39**, 5031 (2000).
[3] F. A. Jenkins and H. A. White, *Fundamentals of Optics* (McGraw-Hill, New York, 1957).
[4] J. Simpson, R. F. Adler, and G. R. North, Bull. Am. Meterol. Soc. **69**, 278 (1988).
[5] R. C. Srivastava, J. Atmos. Sci. **28**, 410 (1971).
[6] T. B. Low and R. List, J. Atmos. Sci. **39**, 1591 (1982).
[7] T. B. Low and R. List, J. Atmos. Sci. **39**, 1607 (1982).
[8] K. Andsager, K. V. Beard, and N. F. Laird, J. Atmos. Sci. **56**, 2673 (1999).
[9] A. Tokay and K. V. Beard, J. Appl. Meteorol. **35**, 1671 (1996).
[10] K. V. Beard, H. T. Ochs, and R. J. Kubesh, Nature (London) **342**, 408 (1989).
[11] K. V. Beard and A. Tokay, Geophys. Res. Lett. **18**, 2257 (1991).
[12] R. J. Doviak and D. S. Zrnić, *Doppler Radar and Weather Observations* (Academic, Orlando, 1984).
[13] J. Joss and A. Waldvogel, Pure Appl. Geophys. **68**, 240 (1967).
[14] J. Joss and A. Waldvogel, J. Appl. Meteorol. **16**, 112 (1977).
[15] M. Schonhuber *et al.*, in Proceedings of Atmospheric Physics and Dynamics in the Analysis and Prognosis of Precipitation Fields, SIMA, Rome, 1994.
[16] M. Schonhuber *et al.*, in Proceedings of the Third International Symposium on Hydrological Applications of Weather Radars, Sao Paulo, Brazil, 1995.
[17] T. J. Schuur and A. V. Rhyzhkov, J. Appl. Meteorol. **40**, 1019 (2001).
[18] V. Chandrasekar, W. A. Cooper, and V. N. Bringi, J. Atmos. Sci. **45**, 1323 (1988).
[19] S. E. Yuter and R. A. Houze, Jr., J. Appl. Meteorol. **36**, 847 (1997).
[20] L. F. Bliven, J. Atmos. Ocean Tech. (in preparation).
[21] E. Fantini, L. Tognotti, and A. Tonazzini, Comput. Chem. Eng. **14**, 1201 (1990).
[22] G. J. Zhang and M. Ishii, Int. J. Heat Mass Transf. **38**, 2019 (1995).
[23] Y. Murai, Y. Matsumoto, and F. Yamamoto, Exp. Fluids **30**, 11 (2001).
[24] N. Chigier, Prog. Energy Combust. Sci. **9**, 155 (1983).
[25] N. Chigier, Atomiz. Spray Technol. **2**, 257 (1986).